

Effects of disturbance on detonation initiation in $H_2/O_2/N_2$ mixtureYuan Wang,¹ Wang Han,^{1,*} Ralf Deiterding,² and Zheng Chen^{1,3,†}¹*CAPT, SKLTCS, College of Engineering, Peking University, Beijing 100871, China*²*Aerodynamics and Flight Mechanics Research Group, University of Southampton, Highfield Campus, Southampton SO171BJ, United Kingdom*³*Beijing Innovation Center for Engineering Science and Advanced Technology, Peking University, Beijing 100871, China*

(Received 10 October 2018; published 20 December 2018)

Detonation initiation has been extensively investigated in the past several decades. In the literature, there are many studies on detonation initiation using a large amount of blast energy and obstacles to respectively achieve direct detonation initiation or deflagration to detonation transition (DDT). However, there are few studies on detonation initiation with a nonuniform initiation zone. In this work, two-dimensional numerical simulations considering detailed chemistry and transport are conducted to investigate the effects of disturbance on detonation initiation in a stoichiometric $H_2/O_2/N_2$ mixture. The high-pressure and high-temperature detonation initiation regime is imposed by a sinusoidal disturbance. Introduction of such disturbance is found to promote the onset of detonation and to reduce time and distance for detonation formation. This is mainly because such disturbance can induce shock-wave interaction, which generates transverse waves. The reflected transverse waves result in local autoignition and explosion. The coherent coupling between local autoignition and pressure wave resulting from a large amount of heat release eventually leads to the detonation development. It is found that the distance and duration for detonation initiation become shorter when a disturbance with smaller wavelength or larger amplitude is enforced. When the ratio between the wavelength and amplitude of disturbance is fixed, the change in wavelength and amplitude has little influence on detonation initiation. Therefore, disturbance with either small wavelength or large amplitude can be used to promote detonation initiation.

DOI: [10.1103/PhysRevFluids.3.123201](https://doi.org/10.1103/PhysRevFluids.3.123201)**I. INTRODUCTION**

Detonation initiation is a fundamental combustion problem, which is related to the development of high-performance detonation engines and the control of accidental explosion. Generally, there are two ways to form a detonation. One is referred to as direct or blast detonation initiation [1–4], in which a large energy source is deposited rapidly into the combustible mixture to directly initiate detonation. The other is deflagration to detonation transition (DDT) [5–10], which involves the acceleration of a flame through obstacles and/or turbulence. No matter which way is used to achieve detonation initiation, both the disturbance and instability development play important roles during detonation initiation [8,11]. Therefore, many studies investigated the influence of these factors on detonation initiation.

*Current address: STFS, TU Darmstadt, Germany.

†Corresponding author: cz@pku.edu.cn

Chue *et al.* [12] conducted one-dimensional simulations to study how periodic longitudinal perturbations in density affect detonation development. They found that the frequency of the applied perturbation plays an important role in the formation of detonation. In their one-dimensional (1D) simulations, Mazaheri [13] and Ng and Lee [14] found that local density disturbance can promote the onset of detonation due to the amplification of local disturbance or instability. Qi and Chen [15] assessed the effects of local temperature perturbation on 1D direct detonation initiation. They found that a cold spot can promote direct detonation initiation. Such unexpected observation was shown to be caused by the opposite effects of temperature perturbation: a locally low temperature reduces the chemical reaction rate while it also increases the local volumetric energy density when the pressure remains unchanged [15]. Radulescu *et al.* [16] examined the influence of cellular instability on the direct initiation of 2D weakly unstable detonations. Their results indicate that multidimensional perturbations and cellular instabilities inhibit the initiation of inviscid detonations. Ng *et al.* [11] noticed that a large wavelength of perturbation was used by Radulescu *et al.* [16] and thereby they examined the effects of perturbation wavelength and channel size on the direct initiation of 2D weakly unstable detonations. They found that high-frequency, small-amplitude perturbations can generate fine-scale instabilities which can accelerate the heat-release rate and thereby promote the onset of detonation [11].

Besides detonation initiation, there are many studies on detonation propagation in spatially inhomogeneous mixtures. Li *et al.* [17] examined the effects of 2D spatial heterogeneity on the near-limit propagation of a pressure-dependent detonation. They found that the spatial heterogeneity enables the detonation wave to propagate at near-limit conditions at greater velocities and in thinner layers than the corresponding homogeneous case. Mi *et al.* [18–20] studied the effect of spatial discretization of energy on detonation propagation. They found that the average detonation wave speeds in a spatially inhomogeneous reactive medium are significantly greater than the corresponding Chapman-Jouguet (CJ) speed of the homogeneous reactive medium. It is noted that there are many studies on DDT caused by obstacles, boundary layers, and turbulence, for which the readers are referred to the review paper [8] and references therein.

One-step chemistry was used in most of the previous studies mentioned above. However, as demonstrated by Body [13] and emphasized by Lee and Higgins [21], successful detonation initiation can always be achieved due to the absence of the crossover temperature in a one-step chemistry model. One-step chemistry cannot predict a distinct value for the critical initiation energy below which no detonation occurs and it therefore has limitations in the study of detonation initiation. Besides, Radulescu and co-workers [22,23] found that physical diffusion needs to be considered for simulating detonation with irregular structure. Hence, in the present study, a detailed chemical mechanism for hydrogen oxidation with 9 species and 25 elementary reactions [24] and the full reactive Navier-Stokes equations are considered in simulating detonation initiation in an $\text{H}_2/\text{O}_2/\text{N}_2$ mixture.

The objective of this study is to investigate the influence of disturbance of detonation initiation region on the detonation initiation process. Two-dimensional numerical simulations with adaptive mesh refinement are conducted, and detailed chemistry and transport are considered. The detonation is initiated by a region with high temperature and pressure. The detonation initiation regime is imposed by a sinusoidal disturbance, and the influence of the wavelength and amplitude of the disturbance on detonation initiation is examined. In addition, the influence of the ratio of wavelength and amplitude of the disturbance on detonation initiation is also investigated.

II. NUMERICAL MODEL AND METHODS

We consider 2D detonation initiation in a $\text{H}_2/\text{O}_2/\text{N}_2$ mixture. The numerical setup is sketched in Fig. 1. Initially, a static stoichiometric H_2/O_2 mixture with 70% (in volume) nitrogen dilution (i.e., the molar ratio is $\text{H}_2 : \text{O}_2 : \text{N}_2 = 2 : 1 : 7$) is uniformly distributed in the whole computational domain. To initiate detonation, a thin region ($0 \leq x \leq 1$ cm) with high temperature and pressure ($T_L = 800$ K, $P_L = 50$ atm) is placed on the left side. The mixture on the right side is at

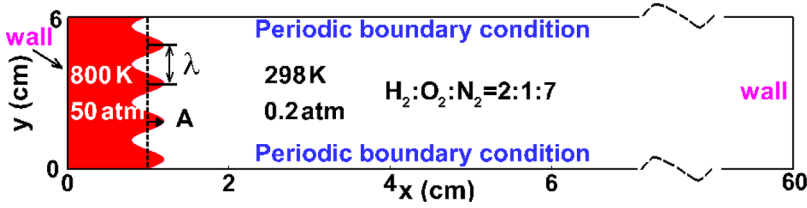


FIG. 1. Schematic of the initial and boundary conditions used in the simulation of detonation initiation in $\text{H}_2/\text{O}_2/\text{N}_2$ mixture. A sinusoidal perturbation with the amplitude of A and wavelength of λ is introduced to the surface of the detonation initiation region at $x = 1$ cm.

$T_R = 298$ K and $P_R = 0.2$ atm. Disturbance is introduced to the surface of the detonation initiation region at $x = 1$ cm. A sinusoidal perturbation with the amplitude of A and wavelength of λ is imposed along the y direction. To investigate the effect of disturbance on detonation initiation, here we change the wavelength λ from 1 mm to infinity (i.e., $\lambda = \infty$, which is equivalent to the case without disturbance) and amplitude A from 1 to 6 mm.

As indicated in Fig. 1, an adiabatic no-slip wall boundary condition is used for the left and right sides of the computational domain. For the top and bottom sides of the computational domain, a periodic boundary condition is used to exclude the influence of wall boundary layers on the detonation initiation and development [25].

The parallel block-structured mesh refinement framework AMROC [26] is used for simulation. AMROC solves the Navier-Stokes equations for unsteady, 2D, multicomponent, compressible reactive flows using the second-order accurate monotonic upwind scheme for conservation laws (MUSCL)-Hancock finite-volume scheme. A hybrid Roe-Harten-Lax-van Leer (HLL) Riemann solver for mixtures of thermally perfect gases is used to calculate the convective fluxes. A second-order accurate central difference scheme is used for multispecies diffusion terms. A semi-implicit Runge-Kutta method of fourth order is adopted to integrate stiff reaction terms and coupled to the finite-volume transport scheme via Godunov splitting. A target Courant-Friedrichs-Lewy (CFL) number of 0.98 is used together with dynamic time-step adjustment. This efficient and adaptive solver has been extensively validated for supersonic combustion and detonation problems [27–30]. More details on governing equations and numerical schemes of AMROC can be found in Ref. [26] and thereby are not represented here.

To accurately and efficiently resolve the detonation initiation process, dynamically adaptive mesh refinement strategy is used in AMROC. Figure 2 shows an example of the initial adaptive mesh distribution. The gradients of temperature, density, and pressure are used to control the adaptive mesh refinement and coarsening. The mesh size before refinement is $0.5 \times 0.5 \text{ mm}^2$. After five level mesh refinement, the finest mesh size is $15.6 \times 15.6 \mu\text{m}^2$. The induction length for a Chapman-Jouguet Zeldovich-von Neumann-Döring (CJ ZND) detonation profile in the present mixture $\text{H}_2/\text{O}_2/\text{N}_2$ at $T_R = 298$ K and $P_R = 0.2$ atm is around 0.63 mm, and thereby it is covered

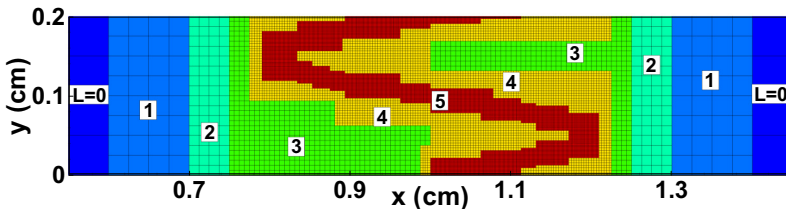


FIG. 2. Distribution of the initial adaptive mesh for the case of $A = 2$ mm and $\lambda = 2$ mm. The number shows the mesh level L and the corresponding mesh size is equal to $500/2^L \mu\text{m}$.

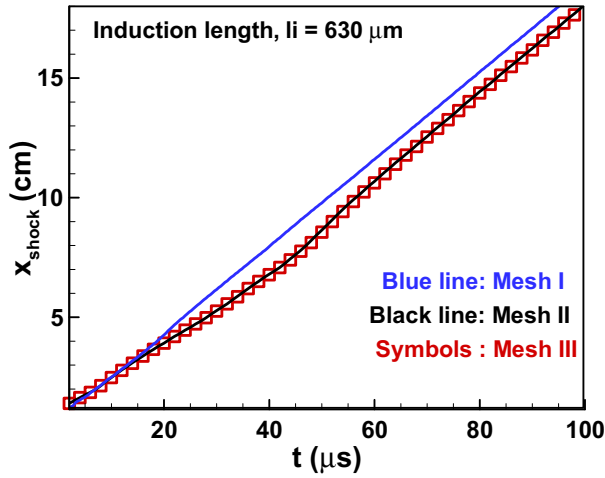


FIG. 3. Shock-wave trajectories during detonation initiation and propagation processes predicted by simulations using different mesh level for $\lambda = 15$ mm and $A = 2$ mm. The coarsest mesh size is fixed at $\Delta x = 500 \mu\text{m}$. The maximum mesh level for mesh I, II, and III are, respectively, $L = 4, 5,$ and 6 . The finest mesh size is equal to $\Delta x/2^L$, which is $31.2, 15.6,$ and $7.8 \mu\text{m}$ for mesh I, II, and III, respectively.

by more than 40 points. Therefore, the detonation is adequately resolved in this study. Besides, grid convergence is ensured through comparison among results from different finest mesh sizes of $31.2, 15.6,$ and $7.8 \mu\text{m}$, as shown in Fig. 3. It is seen that the results by using mesh I (with the finest mesh size of $31.2 \mu\text{m}$) significantly differ from that by using mesh II (with the finest mesh size of $15.6 \mu\text{m}$) and mesh III (with the finest mesh size of $7.8 \mu\text{m}$). This indicates that insufficient resolution affects the detonation initiation. It is observed that the results from mesh II are almost identical to those from mesh III. Therefore, numerical convergence is reached and the finest mesh size of $15.6 \mu\text{m}$ is used in all the simulations.

As additional verification and to demonstrate the validity of the general simulation setup, we compare our computational results with those reported by Oran *et al.* [31] and Wang *et al.* [32]. Specifically, the detonation propagation in hydrogen/oxygen/argon (with molar ratio of $\text{H}_2 : \text{O}_2 : \text{Ar} = 2 : 1 : 7$) mixture at 298 K and 6.67 kPa is simulated. The detonation propagates in a channel with a height of 6 cm, which is the same as that in Refs. [31,32]. The cellular structure is shown in Fig. 4. The cell size is approximately 55×30 mm, which is very close to the values of 54×31 mm and 54×30 mm, respectively, obtained by Oran *et al.* [31] and Wang *et al.* [32]. Meanwhile, the

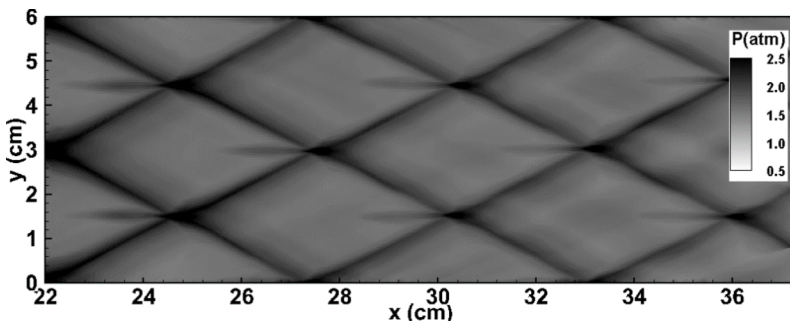


FIG. 4. Numerical soot foils for detonation propagation in $2\text{H}_2 + \text{O}_2 + 7\text{Ar}$ mixture at 298 K and 6.67 KPa.

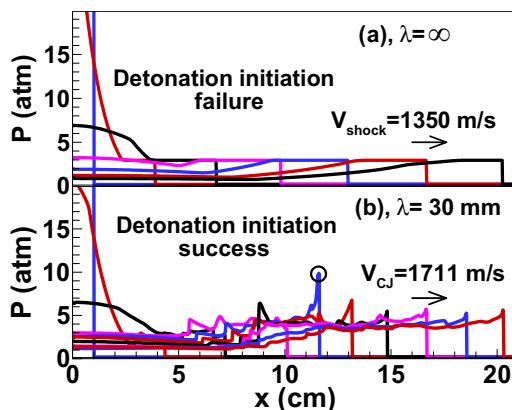


FIG. 5. Temporal evolution of pressure distributions along the fixed line at $y = 1.5$ cm for (a) $\lambda = \infty$ (i.e., without disturbance) and (b) $\lambda = 30$ mm and $A = 2$ mm.

average speed of detonation propagation from our simulation is 1598 m/s, which is close to the values of 1625 and 1595 m/s, respectively, obtained by Oran *et al.* [31] and Wang *et al.* [32]. Therefore, the current 2D numerical simulation can reproduce the results reported in the literature. It is noted that systematic convergence studies for AMROC have been conducted before by Deiterding [33–35]. The readers are referred to these publications for more details.

III. RESULTS AND DISCUSSION

First we consider detonation initiation with fixed amplitude of disturbance $A = 2$ mm. The effects of disturbance on detonation initiation are assessed through comparing results for different wavelengths, λ , of the perturbation located at the surface of detonation initiation region, as indicated in Fig. 1.

Figure 5 shows the temporal evolution of pressure distributions along the fixed line at $y = 1.5$ cm. When there is no disturbance in the initiation region (i.e., $\lambda = \infty$), the leading shock propagates to the right side at the speed of 1350 m/s. The unburned gas is compressed by the leading shock to reach 956 K and 3.3 atm, at which the ignition delay time is about 25 ms. Therefore, autoignition cannot immediately happen and the reaction zone cannot couple with the leading shock. Consequently, detonation initiation fails when no disturbance is introduced to the initiation region. However, when a disturbance is introduced to the initiation region (i.e., $A = 2$ mm and $\lambda = 30$ mm), Fig. 5(b) shows that successful detonation initiation is achieved. As the leading shock propagates to the right side, local autoignition occurs immediately after the leading shock around $x = 7$ cm, which is shown later in Fig. 6(b). The pressure waves generated by heat release accelerate the propagation of the reaction front. At the time of $t = 74 \mu\text{s}$, the leading shock arrives at $x = 11.9$ cm. The reaction zone couples with the leading shock, resulting in an overdriven detonation and the pressure of the leading shock is around 11 atm. Then the overdriven detonation decays and eventually becomes a self-sustained detonation propagating at the CJ velocity of 1711 m/s. Therefore, the above results indicate that the disturbance with the wavelength of $\lambda = 30$ mm can promote the onset of detonation.

Figures 6–9 further show the details on the detonation initiation process with $\lambda = 30$ mm. The evolution of temperature distribution is shown in Fig. 6. At the beginning, a curved leading shock is generated at the right surface of the detonation initiation region with sinusoidal disturbance. As the leading shock waves propagate and interact with each other due to the collision at the symmetry line, $y = \lambda/2 = 15$ mm, and the reflection at the top and bottom sides of periodic boundary, $y = 0$ and $y = \lambda = 30$ mm, local autoignition is triggered around $t = 40 \mu\text{s}$, as shown in Fig. 6(b). Heat release from such nearly constant-volume autoignition can generate a pressure wave, which

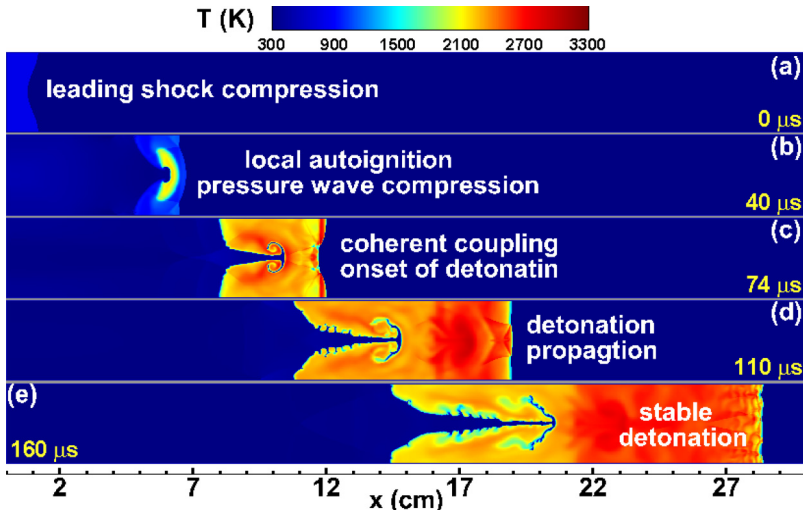


FIG. 6. Evolution of temperature contour for $\lambda = 30$ mm and $A = 2$ mm. For each frame, the vertical height is 30 mm (i.e., $0 \leq y \leq 30$ mm).

further compresses the unburned gas and induces further autoignition. Eventually, coherent coupling between autoignition and pressure wave leads to the detonation development according to the shock-wave amplification by coherent energy release (SWACER) mechanism of Lee *et al.* [36,37]. Figure 7 shows the trajectories of shock wave and reaction front along the fixed line at $y = 1.5$ cm. It is observed that the distance between the leading shock wave and reaction front remains nearly constant for $t < 67 \mu\text{s}$. This corresponds to the so-called quasisteady state, which also occurs in one-dimensional direct detonation initiation (e.g., [15]). Around $t = 67 \mu\text{s}$, the reaction front generated by local autoignition starts to accelerate due to the coupling between autoignition and pressure waves. Eventually, it catches up and merges with the leading shock around $t = 74 \mu\text{s}$,

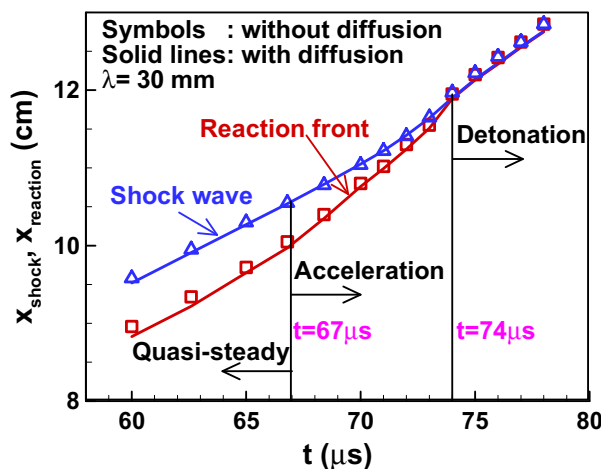


FIG. 7. Evolution of the trajectories of shock wave and reaction front along the fixed line at $y = 1.5$ cm for $\lambda = 30$ mm and $A = 2$ mm. The solid lines are obtained from a simulation including diffusion, while the symbols correspond to the inviscid case.

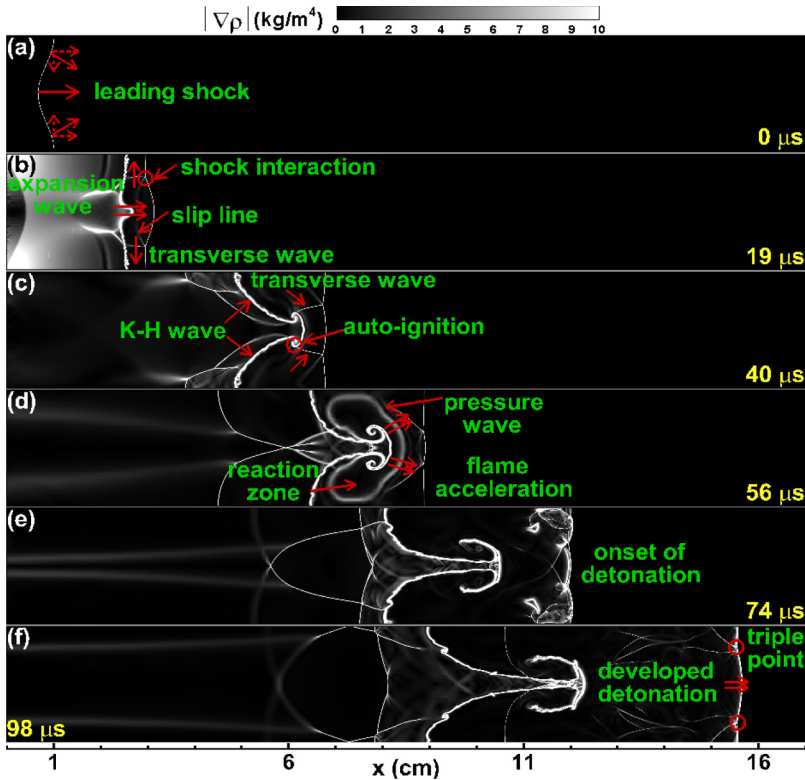


FIG. 8. Evolution of density gradient contour for $\lambda = 30$ mm and $A = 2$ mm.

resulting in a detonation propagating afterwards as shown in Fig. 7. Figure 6(c) shows that the detonation is formed around $x = 11.9$ cm at $t = 74 \mu\text{s}$. Therefore, the detonation development occurs due to the SWACER mechanism [36,37] in which the coherent coupling between heat release and pressure pulse leads to detonation development.

Radulescu and co-workers [22,23] found that physical and numerical diffusion plays an important role on unstable cellular detonations. To quantify the effects of diffusion on detonation initiation, we have also conducted a simulation without considering physical diffusion (i.e., to solve reactive Euler equations instead of reactive Navier-Stokes equations). The comparison shown in Fig. 7 indicates that diffusion transport has little effect on detonation initiation. It is noted that some numerical diffusion always exists. As shown in Fig. 3, the grid convergence is achieved at least in terms of detonation initiation distance.

It is noticed that in the last two frames in Fig. 6, instabilities appear at the interface of hot burned gas and cold unburned gas in which a large difference in density exists. In the present 2D simulation, the vortex stretching effect in the third dimension is not included and thereby the instabilities are not accurately captured. Nevertheless, the shock- and pressure-wave interactions captured in the present 2D simulation do show the promotion of detonation initiation by the perturbation introduced at the surface of the detonation initiation region. Such promotion is expected to be more significant in the 3D case than in the 2D case. This was found by Kuchugov *et al.* [38] who showed that 3D perturbations grow faster than 2D ones in Rayleigh-Taylor instabilities. In 3D cases, the wave collisions increase and so does the number of transverse waves, resulting in more advanced local autoignition and detonation development.

To further interpret the autoignition and detonation initiation, the evolution of density gradient distribution is plotted in Fig. 8. Initially, the curved leading shock is generated due to the pressure discontinuity. Since the shock propagation velocity along the x direction is different for

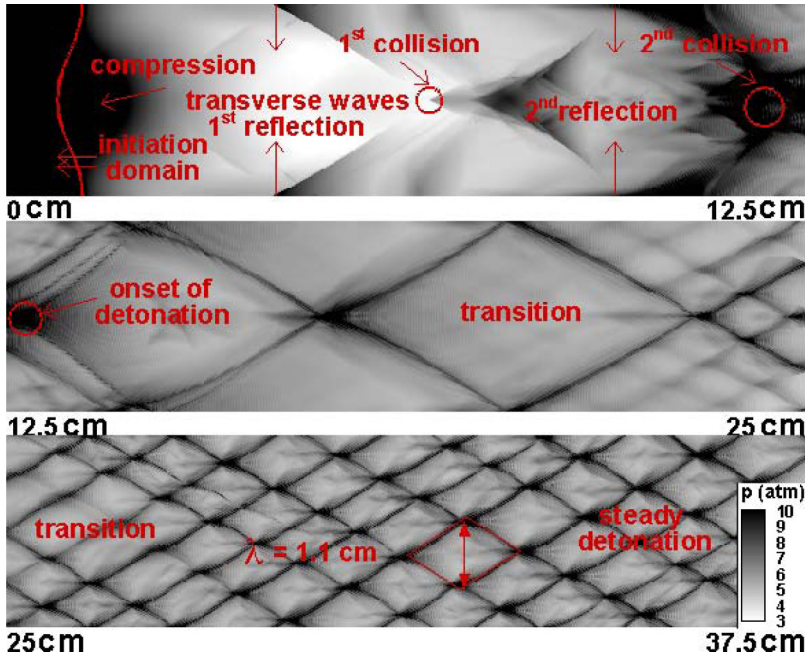


FIG. 9. Numerical soot foils for $\lambda = 30$ mm and $A = 2$ mm. The vertical height is 30 mm.

different parts of the curved leading shock, shock interaction occurs. Around the symmetry line at $y = \lambda/2 = 15$ mm, the strong interaction among shock waves generates transverse waves and slip lines, as indicated in Fig. 8(b). The two transverse waves propagate upward and downward, respectively. The unburned gas has high reactivity after it is compressed by the leading shock and transverse waves. As a result, when the transverse waves are reflected at the symmetric lines, they can further compress unburned gas for a second time, which induces local autoignition, as shown in Figs. 8(c) and 6(b). The local autoignition is confirmed by the fast production of OH radicals. The local autoignition can generate a strong pressure wave, as shown in Fig. 8(d). The pressure wave can then further compress the unburned gas between the leading shock and reaction front and thereby trigger autoignition therein. Consequently, the reaction front propagation accelerates and subsequently catches up and couples with the leading shock, indicating the formation of detonation [see Figs. 8(e) and 6(c) for $t = 74 \mu\text{s}$]. Eventually, the fully developed and self-sustained detonation propagates to the right side at the CJ speed of 1711 m/s [see Figs. 8(f) and 6(e)]. The triple points are generated through the interaction among incident shock, Mach stem, and transverse wave. Regular movement of triple points forms a cellular structure [36], which is the most significant feature of detonation, as shown in Fig. 9 for $x > 25$ cm. However, before the detonation is fully developed, the cell size increases and the big cells (which appear within $12.5 < x < 23$ cm in Fig. 9) are due to the fact that the initial perturbation still affects the movement of triple points and the cellular structure. Simulation results show that the big cell size is proportional to the wavelength of disturbance. For the stage of fully developed and self-sustained detonation propagation, a regular cellular structure is observed in Fig. 9 and the cell size is about 1.1 cm.

The above results are for the disturbance with the wavelength of $\lambda = 30$ mm. We also study detonation initiation with different wavelengths of disturbance. Figure 10 shows the distribution of the density gradient, pressure, and temperature contour for $\lambda = 15$ and $\lambda = 30$ mm at the same time of $t = 15 \mu\text{s}$. Compared to the larger wavelength of $\lambda = 30$ mm without local autoignition at the present time, local autoignition already happens for the smaller wavelength of $\lambda = 15$ mm, which results in a pressure wave after the leading shock. Therefore, with the decrease of the disturbance wavelength, the local autoignition appears earlier and so does the coupling between autoignition

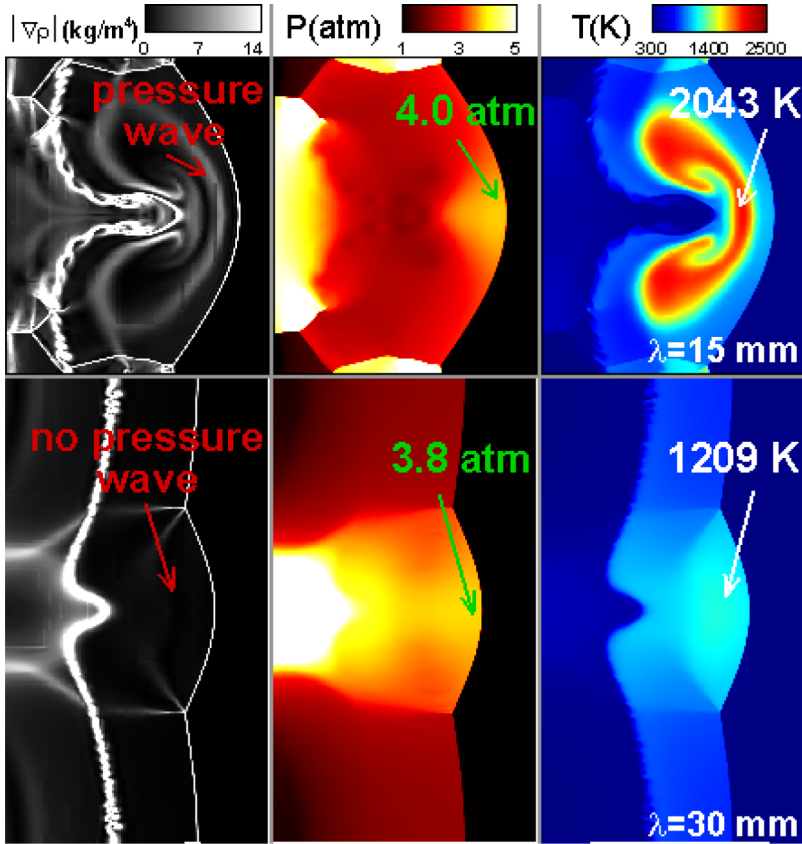


FIG. 10. Density gradient, pressure, and temperature contour. Top: $\lambda = 15$ mm; bottom: $\lambda = 30$ mm. The amplitude is fixed to be $A = 2$ mm.

and pressure waves, which leads to detonation development according to the SWACER mechanism. Consequently, a disturbance with small wavelength can be used to promote detonation initiation.

The results for detonation initiation with different wavelengths of disturbance are summarized in Fig. 11. For $\lambda = \infty$ (i.e., without disturbance), the shock wave propagates at the speed of 1350 m/s and no autoignition happens afterwards. Thereby, detonation initiation fails. For $\lambda = 30$ mm, as discussed above, the detonation forms around $t = 74 \mu\text{s}$, and the propagation speed of the shock wave increases suddenly for $t > 74 \mu\text{s}$. As the wavelength of disturbance is decreased to $\lambda = 15$ mm, the time for detonation development reduces to $42 \mu\text{s}$. This indicates that disturbance with shorter wavelength promotes detonation initiation more efficiently than that with longer wavelength. This is because at fixed amplitude, a shorter wavelength corresponds to larger curvature of the leading shock and thereby stronger shock-wave interaction. This is consistent with results shown in Fig. 10. For $\lambda = 1$ mm, rapid autoignition happens after strong interaction of the leading shock, and the reaction zone can immediately couple to the leading shock wave. Detonation formation only takes $9.5 \mu\text{s}$ for $\lambda = 1$ mm, which is about one order smaller than that of $\lambda = 30$ mm. Therefore, the distance and duration for detonation formation can be greatly reduced through decreasing the disturbance wavelength.

The above results are for disturbances with different wavelengths but fixed amplitude of $A = 2$ mm. We also consider disturbances with different amplitudes but fixed wavelength, for which the results are summarized in Fig. 12. For a small amplitude of $A = 1$ mm, the leading shock is not accelerated since weak interaction of shock wave cannot induce autoignition. Therefore,

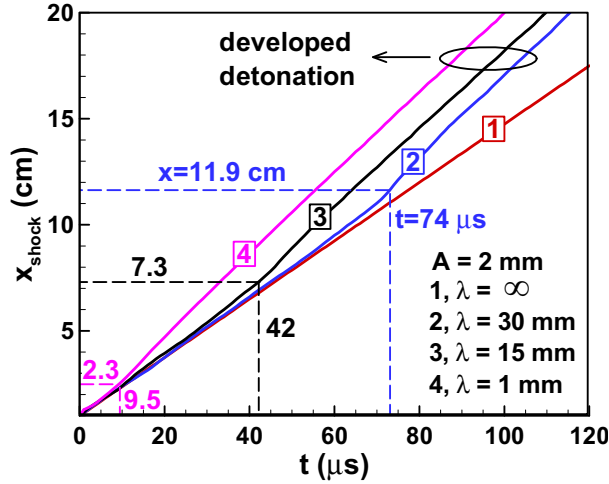


FIG. 11. Evolution of shock-wave trajectories for disturbances with different wavelengths, but fixed amplitude of $A = 2$ mm. The dashed lines indicate the time and position of detonation formation.

detonation initiation fails for $A = 1$ mm. With the increase of the amplitude of the disturbance to $A = 2, 4,$ and 6 mm, successful detonation initiation is achieved. Moreover, the distance and duration of detonation formation both decrease as amplitude increases. Therefore, increasing the amplitude of disturbance can also greatly promote detonation initiation. This is reasonable since at fixed wavelength, larger amplitude corresponds to higher curvature of the leading shock and thereby stronger shock-wave interaction.

Figure 13 shows the change of the leading shock pressure with the shock position for disturbances with different amplitudes but fixed wavelength of $\lambda = 30$ mm. For $A = 2$ mm, there are two peaks of shock pressure, which correspond to the double collisions of transverse waves. At the location of the second peak of shock pressure, an overdriven detonation develops with the peak pressure being around two times the pressure of the von Neumann spike. During its propagation,

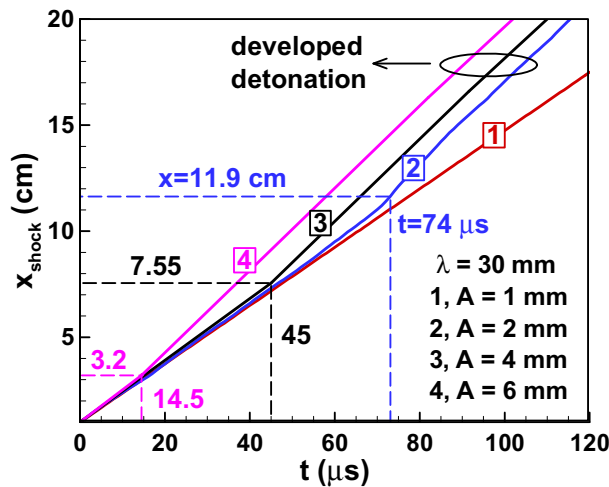


FIG. 12. Evolution of shock-wave trajectories for disturbances with different amplitudes, but fixed wavelength of $\lambda = 30$ mm. The dashed lines indicate the time and position of detonation formation.

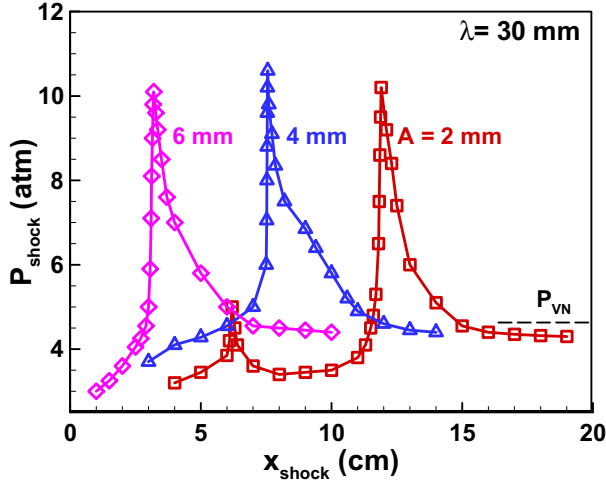


FIG. 13. Change of the leading shock pressure P_{shock} with the shock position X_{shock} along the line at $y = 1.5$ cm for disturbances with fixed wavelength of $\lambda = 30$ mm, but different amplitudes of $A = 2, 4,$ and 6 mm.

the overdriven detonation decays and it eventually becomes a self-sustained propagating detonation with shock pressure being close to the pressure of the von Neumann spike. For $A = 4$ mm, only one peak of shock pressure appears when the shock arrives at $X_{\text{shock}} = 7.55$ cm, which corresponds the one collision of transverse waves. However, the larger amplitude of disturbance generates stronger shock-wave interaction. Thereby, the distance for detonation formation is reduced. For even larger amplitude of $A = 6$ mm, the distance for detonation formation is shown to be further reduced to $X_{\text{shock}} = 3.2$ cm.

The influence of wavelength and amplitude of disturbance on the distance for detonation formation is summarized in Fig. 14. When the amplitude of disturbance is fixed to be $A = 2$ mm, Fig. 14(a) shows that the distance for detonation formation increases almost linearly with the wavelength of disturbance. When the wavelength of the disturbance is fixed to be $\lambda = 30$ mm, Fig. 14(b) indicates that the distance for detonation formation decreases almost linearly with the amplitude of disturbance. Finally, when the ratio between the wavelength and amplitude of disturbance is fixed to be $\lambda/A = 15$, the distance for detonation formation remains nearly constant. These trends are reasonable since the wavelength and amplitude determine the shape (or curvature) of the initial shock and the intensity of subsequent shock-wave interaction. The above results indicate that in order to efficiently promote detonation initiation, a disturbance with small wavelength or large amplitude can be used.

IV. CONCLUSIONS

Two-dimensional numerical simulations are conducted to study detonation initiation in $\text{H}_2/\text{O}_2/\text{N}_2$ mixtures. Detailed chemistry and transport are considered and block-structured adaptive mesh refinement is used to efficiently resolve the detonation development. A disturbance is introduced on the surface of high-pressure and high-temperature initiation region. Periodic boundary conditions are used for the top and bottom sides of the computational domain. The influence of disturbance on detonation initiation is examined. It is observed that the disturbance can induce complex shock-wave interaction, which generates transverse waves propagating in opposite directions. It is the reflected transverse waves that trigger local autoignition and explosion. The coherent coupling between local autoignition and pressure wave leads to detonation development. With the decrease of the disturbance wavelength or increase of the disturbance amplitude, the shock-wave interaction

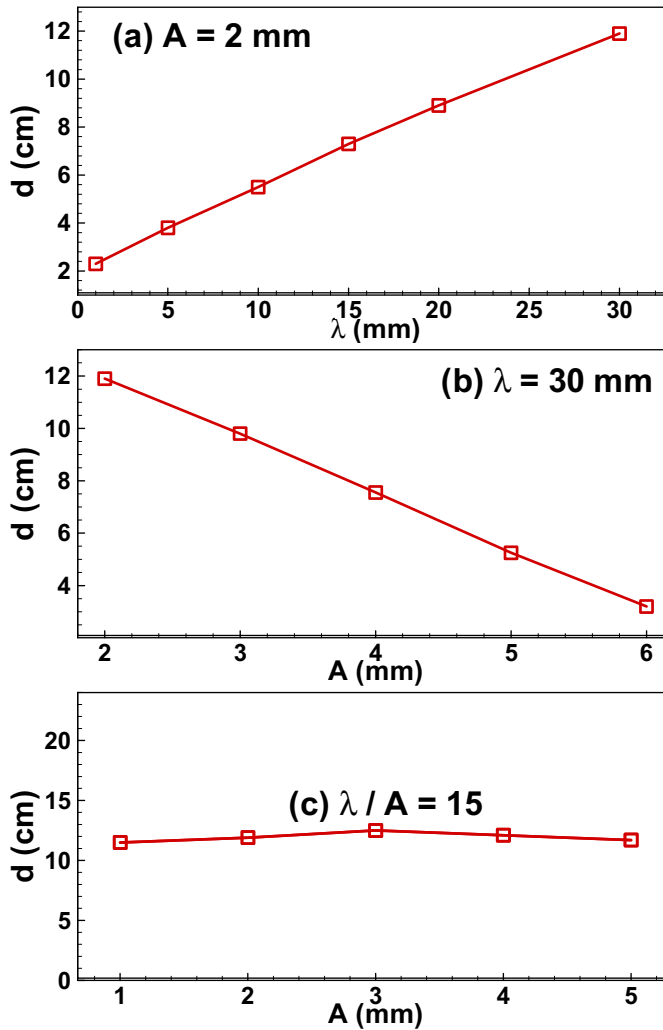


FIG. 14. Change of the distance for detonation formation with wavelength or amplitude of the disturbance.

becomes stronger and thereby the distance and duration for detonation initiation become shorter. However, proportional change in wavelength and amplitude (i.e., their ratio is fixed) does not lead to the obvious change in the distance and duration for detonation initiation are almost constant. Therefore, disturbance with either small wavelength or large amplitude helps to promote detonation initiation.

ACKNOWLEDGMENTS

This work was supported by the National Natural Science Foundation of China (Grants No. 91741126 and No. 91541204). We are grateful for helpful discussions with Professor Hoi Dick Ng at Concordia University, Professor Matei I. Radulescu at University of Ottawa, and Dr. Wenhua Han at Beijing Institute of Technology. The simulations were conducted on the High Performance Computing Platform of the Center for Life Science at Peking University and on the Tianhe-2A supercomputer in Guangzhou, China.

- [1] H. D. Ng and J. H. S. Lee, Direct initiation of detonation with a multi-step reaction scheme, *J. Fluid Mech.* **476**, 179 (2003).
- [2] B. Zhang, V. Kamenskihs, H. D. Ng, and J. H. S. Lee, Direct blast initiation of spherical gaseous detonations in highly argon diluted mixtures, *Proc. Combust. Inst.* **33**, 2265 (2011).
- [3] V. Kamenskihs, H. D. Ng, and J. H. S. Lee, Measurement of critical energy for direct initiation of spherical detonations in stoichiometric high-pressure H₂-O₂ mixtures, *Combust. Flame* **157**, 1795 (2010).
- [4] C. A. Eckett, J. J. Quirk, and J. E. Shepherd, The role of unsteadiness in direct initiation of gaseous detonations, *J. Fluid Mech.* **421**, 147 (2000).
- [5] V. N. Gamezo, T. Ogawa, and E. S. Oran, Flame acceleration and DDT in channels with obstacles: Effect of obstacle spacing, *Combust. Flame* **155**, 302 (2008).
- [6] G. I. Sivashinsky, Some developments in premixed combustion modeling, *Proc. Combust. Inst.* **29**, 1737 (2002).
- [7] S. B. Dorofeev, Flame acceleration and explosion safety applications, *Proc. Combust. Inst.* **33**, 2161 (2011).
- [8] E. S. Oran and V. N. Gamezo, Origins of the deflagration-to-detonation transition in gas-phase combustion, *Combust. Flame* **148**, 4 (2007).
- [9] G. Ciccarelli and S. Dorofeev, Flame acceleration and transition to detonation in ducts, *Prog. Energy Combust. Sci.* **34**, 499 (2008).
- [10] E. S. Oran, Understanding explosions—From catastrophic accidents to creation of the universe, *Proc. Combust. Inst.* **35**, 1 (2015).
- [11] H. D. Ng, C. B. Kiyanda, G. H. Morgan, and N. Nikiforakis, The influence of high-frequency instabilities on the direct initiation of two-dimensional gaseous detonations, in *25th International Colloquium on the Dynamics of Explosions and Reactive Systems, Leeds, UK* (2015).
- [12] R. S. Chue, J. H. S. Lee, and F. Zhang, Transition from fast deflagration to detonation under the influence of periodic longitudinal perturbations, *Shock Waves* **5**, 159 (1995).
- [13] K. Mazaheri, Mechanism of the onset of detonation in blast initiation, Ph.D. thesis, McGill University, 1997.
- [14] H. D. Ng and J. H. S. Lee, The influence of local disturbances on the direct initiation of detonations, in *18th International Colloquium on the Dynamics of Explosions and Reactive Systems, Seattle, USA* (2001).
- [15] C. Qi and Z. Chen, Effects of temperature perturbation on direct detonation initiation, *Proc. Combust. Inst.* **36**, 2743 (2017).
- [16] M. I. Radulescu, G. J. Sharpe, and C. K. Law, Effect of cellular instabilities on the blast initiation of weakly unstable detonations, in *21st International Colloquium on the Dynamics of Explosions and Reactive Systems, Poitiers, France* (2007).
- [17] J. Li, X. Mi, and A. J. Higgins, Effect of spatial heterogeneity on near-limit propagation of a pressure-dependent detonation, *Proc. Combust. Inst.* **35**, 2025 (2015).
- [18] X. Mi, A. J. Higgins, H. D. Ng, C. B. Kiyanda, and N. Nikiforakis, Propagation of gaseous detonation waves in a spatially inhomogeneous reactive medium, *Phys. Rev. Fluids* **2**, 053201 (2017).
- [19] X. Mi, E. V. Timofeev, and A. J. Higgins, Effect of spatial discretization of energy on detonation wave propagation, *J. Fluid Mech.* **817**, 306 (2017).
- [20] X. Mi, A. J. Higgins, C. B. Kiyanda, H. D. Ng, and N. Nikiforakis, Effect of spatial inhomogeneities on detonation propagation with yielding confinement, *Shock Waves* **28**, 993 (2018).
- [21] J. H. S. Lee and A. J. Higgins, Comments on criteria for direct initiation of detonation, *Philos. Trans. R. Soc. London A: Math. Phys. Eng. Sci.* **357**, 3503 (1999).
- [22] M. I. Radulescu, A detonation paradox: Why inviscid detonation simulations predict the incorrect trend for the role of instability in gaseous cellular detonations, *Combust. Flame* **195**, 151 (2018).
- [23] K. Mazaheri, Y. Mahmoudi, and M. I. Radulescu, Diffusion and hydrodynamic instabilities in gaseous detonations, *Combust. Flame* **159**, 2138 (2012).
- [24] J. Li, Z. Zhao, A. Kazakov, and F. L. Dryer, An updated comprehensive kinetics model of hydrogen combustion, *Int. J. Chem. Kinet.* **36**, 566 (2004).
- [25] W. Han, Y. Gao, and C. K. Law, Flame acceleration and deflagration-to-detonation transition in micro- and macro-channels: An integrated mechanistic study, *Combust. Flame* **176**, 285 (2017).

- [26] R. Deiterding, Block-structured adaptive mesh refinement-theory, implementation and application, *Esaim: Proc.* **34**, 97 (2011).
- [27] R. Deiterding, A parallel adaptive method for simulating shock-induced combustion with detailed chemical kinetics in complex domains, *Comput. Struct.* **87**, 769 (2009).
- [28] R. Deiterding, High-resolution numerical simulation and analysis of Mach reflection structures in detonation waves in low-pressure H_2 - O_2 -Ar mixtures: A summary of results obtained with the adaptive mesh refinement framework AMROC, *J. Combust.* **2011**, 738969 (2011).
- [29] X. Cai, J. Liang, and R. Deiterding, Numerical investigation on detonation control using a pulse hot jet in supersonic combustible mixture, *Combust. Sci. Technol.* **188**, 1674 (2016).
- [30] X. Cai, J. Liang, R. Deiterding, and Z. Lin, Detonation simulations in supersonic combustible mixtures with nonuniform species, *AIAA J.* **54**, 2449 (2016).
- [31] E. S. Oran, J. W. Weber, E. I. Stefaniw, M. H. Lefebvre, and J. D. Anderson, A numerical study of a two-dimensional H_2 - O_2 -Ar detonation using a detailed chemical reaction model, *Combust. Flame* **113**, 147 (1998).
- [32] C. J. Wang, S. L. Xu, and C. M. Guo, Gaseous detonation propagation in a bifurcated tube, *J. Fluid Mech.* **599**, 81 (2008).
- [33] R. Deiterding, Parallel adaptive simulation of multi-dimensional detonation structures, Ph.D. thesis, Brandenburgische Technische Universität Cottbus, 2003.
- [34] R. Deiterding, Detonation structure simulation with AMROC, in *High Performance Computing and Communications*, Lecture Notes in Computer Science Vol. 3726 (Springer, Berlin, Heidelberg, 2005), pp. 916–927.
- [35] R. Deiterding, A high-resolution method for realistic detonation structure simulation, in *Proc. Tenth Int. Conf. Hyperbolic Problems*, edited by W. Takahashi and I. Tanaka (Yokohama Publishers, Yokohama, Japan, 2006), Vol. 1, pp. 343–350.
- [36] J. H. S. Lee, *The Detonation Phenomenon* (Cambridge University Press, Cambridge, 2008).
- [37] J. H. S. Lee, R. Knystautas, and N. Yoshikawa, Photochemical initiation of gaseous detonations, *Acta Astronaut.* **5**, 971 (1978).
- [38] P. A. Kuchugov, V. B. Rozanov, and N. V. Zmitrenko, The differences in the development of Rayleigh-Taylor instability in 2d and 3d geometries, *Plasma Phys. Rep.* **40**, 451 (2014).